J. Synchrotron Rad. (2000). **7**, 326–332

Enhancement of the spin-dependent effect of $\pi/2$-angle Compton scattering using elliptically polarized synchrotron radiation

N. Sakai,* M. Seigo, Y. Kakutani, N. Hiraoka and A. Koizumi

Department of Material Science, Himeji Institute of Technology, 3-2-1 Kouto, Kamigori, Ako-gun, Hyogo 678-1297, Japan. E-mail: n_sakai@sci.himeji-tech.ac.jp

(*Received 8 November 1999; accepted 5 May 2000*)

Noticeable enhancement of the spin-dependent Compton scattering intensity in right-angle scattering has been achieved by using high-energy X-rays having elliptical polarization. A promising momentum resolution of better than 0.4 atomic units for Compton-profile measurements is firmly predicted by means of an ordinary Ge solid-state detector when the scattering-angle divergence at 90° is crucially restricted. It is pointed out that the angle between a scattering vector and the direction of sample magnetization can be chosen as 90° without seriously weakening the spin-dependent effect. Comparison is made between 274 keV and 122 keV experiments.

Keywords: Compton profiles; spin-dependent scattering; electron momentum density.

1. Introduction

The presence of a magnetic interaction between the electromagnetic field and the electron orbital currents and intrinsic spins makes synchrotron radiation one of the most useful tools for the study of magnetism. Many theoretical and experimental studies have been carried out and valuable information has been obtained. The magnetic interaction, however, is weak in comparison with the charge interaction, except for some resonance magnetic absorption and scattering. In the case of Compton scattering on ordinary ferromagnetic samples, the magnetic effect contributes to, at most, a few percent of the total scattering intensity for circularly polarized photons. This limitation has been improved to some extent by adopting right-angle scattering geometry (RSG), in which the charge scattering is greatly suppressed, as described below. RSG has been commonly adopted in magnetic Bragg-diffraction experiments for the same purpose (Brunel *et al.*, 1983; Ito & Hirano, 1997).

An energy spectrum of Compton-scattered photons in a fixed direction (Compton profile) contains valuable information on the momentum distribution of electrons in matter. Hitherto, Compton profiles have been measured by using the backscattering geometry (BSG). This is based on the fact that, firstly, the Doppler effect on the scattered photons is large and, secondly, the scattering-angle divergence does not affect the momentum resolution of the Compton profile very much, and thus BSG gives a good counting efficiency. In addition, the spin-dependent Compton-scattering cross section is large for BSG. After utilizing high-energy and high-flux synchrotron radiation emitted from a low-emittance storage ring, like at the ESRF and SPring-8, it has been recognized that these advantages of BSG (McCarthy *et al.*, 1997) are also fulfilled by RSG. The present paper reports a noticeable enhancement of the magnetic effect on the spin-dependent Compton profile of Fe of up to 3.4% with a reasonable momentum resolution of 0.5 atomic units (a.u.) by using an ordinary Ge solid-state detector (SSD) as an energy analyzer.

2. Theoretical analysis

The differential scattering cross section for Compton scattering for electrons at rest can be written as (Lipps & Tolhoek, 1954)

$$\begin{aligned}
&\frac{\mathrm{d}\sigma}{\mathrm{d}\Omega} = r_0^2\left(\frac{k^2}{k_0^2}\right)\left[\Phi_0 + P_L\Phi_1 + P_C\Phi_2\right],\\
&\Phi_0(\theta, E_0, E) = (1/8)\left[(1+\cos^2\theta) + \frac{E_0 - E}{mc^2}(1-\cos\theta)\right],\\
&\Phi_1(\theta) = (1/8)\sin^2\theta,\\
&\Phi_2(\theta, \mathbf{k}_0, \mathbf{k}, \boldsymbol{\sigma}) = (1/8)(1-\cos\theta)\boldsymbol{\sigma}\cdot\frac{\hbar}{mc}(\mathbf{k}_0\cos\theta + \mathbf{k}),
\end{aligned} \tag{1}$$

where r_0 denotes the electromagnetic radius of the electron, $\mathbf{k}_0$ and E_0 ($\mathbf{k}$ and E) the wave number and energy of the incident (scattered) photons, respectively, $\boldsymbol{\sigma}$ the unit vector parallel to the direction of the electron spin, and θ the scattering angle.

Here we define a figure of merit $f(\theta_1, \theta_2, \theta)$, which is adequate to optimize the relative intensity of the spin-dependent Compton scattering with respect to the total scattering intensity. The following relation expresses the

signal-to-noise ratio as a function of the Stokes parameters P_L and P_C, the flux density $N_{\rm ph}$ of emitted photons, and the vertical width of the front-end slit represented by angles θ_1 and θ_2,

$$f(\theta_1, \theta_2, \theta) = \Phi_2(\theta, \mathbf{k}_0, \mathbf{k}, \boldsymbol{\sigma}) \int_{-\infty}^{\infty} \mathrm{d}\theta_x \int_{\theta_2}^{\theta_1} N_{\rm ph}(\theta_x, \theta_y) P_C(\theta_x, \theta_y)\, \mathrm{d}\theta_y \Big/ \Big\{ \int_{-\infty}^{\infty} \mathrm{d}\theta_x \int_{\theta_2}^{\theta_1} N_{\rm ph}(\theta_x, \theta_y) \times \big[\Phi_0(\theta, E_0, E) + P_L(\theta_x, \theta_y)\Phi_1(\theta)\big]\, \mathrm{d}\theta_y \Big\}^{1/2}. \quad (2)$$

Here θ_x and θ_y are horizontal and vertical angles, respectively, of the photons as shown in Fig. 1. The denominator expresses the noise, which is the statistical error of the total number of scattered photons. When the photon flux is low, as in the case for 274 keV X-rays, we are forced to use a wide slit and optimize the slit width with parameters $\theta_1 = \theta_H$ and $\theta_2 = -\theta_H$. On the other hand, when the incident flux density is high, as in the case for 122 keV X-rays, we are able to make the front-end slit narrow ($\theta_1 \simeq \theta_2$) to obtain the best condition. For photons of a few hundred keV, a scattering angle of 90° promises to reduce the denominator of (2), and the f factor for a low photon flux is proportional to

$$h(\theta_H, -\theta_H, 90) = \int_{-\infty}^{\infty} d\theta_x \int_{0}^{\theta_H} N_{\rm ph}(\theta_x, \theta_y) P_C(\theta_x, \theta_y)\, \mathrm{d}\theta_y \Big/ \Big\{ \int_{-\infty}^{\infty} \mathrm{d}\theta_x \int_{0}^{\theta_H} N_{\rm ph}(\theta_x, \theta_y) \big[1 + P_L(\theta_x, \theta_y) + (E_0 - E)/mc^2\big]\, \mathrm{d}\theta_y \Big\}^{1/2}. \quad (3)$$

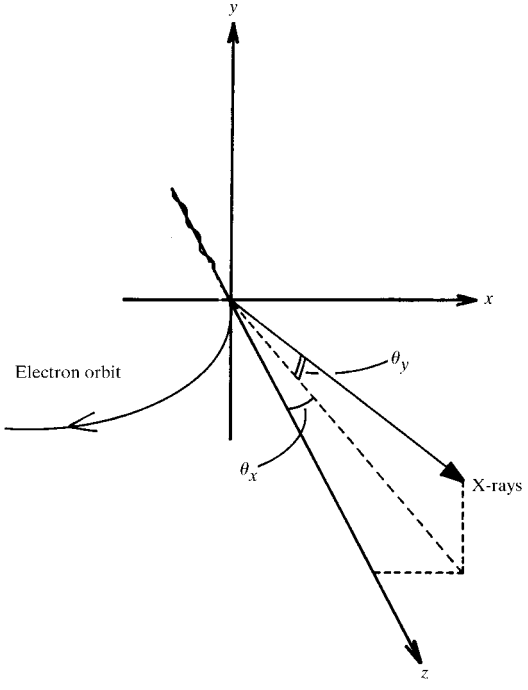

Figure 1
Definition of θ_x and θ_y of emitted X-rays.

This is a complex function of θ_H, because P_C, P_L and $N_{\rm ph}$ have a distribution in space as shown in Figs. 2(a) and 2(b). The parameter K_x is proportional to the horizontal magnetic field intensity of a wiggler. This field is necessary for producing circularly polarized photons, and induces a twin-peaked flux-density distribution of the X-rays. P_C is

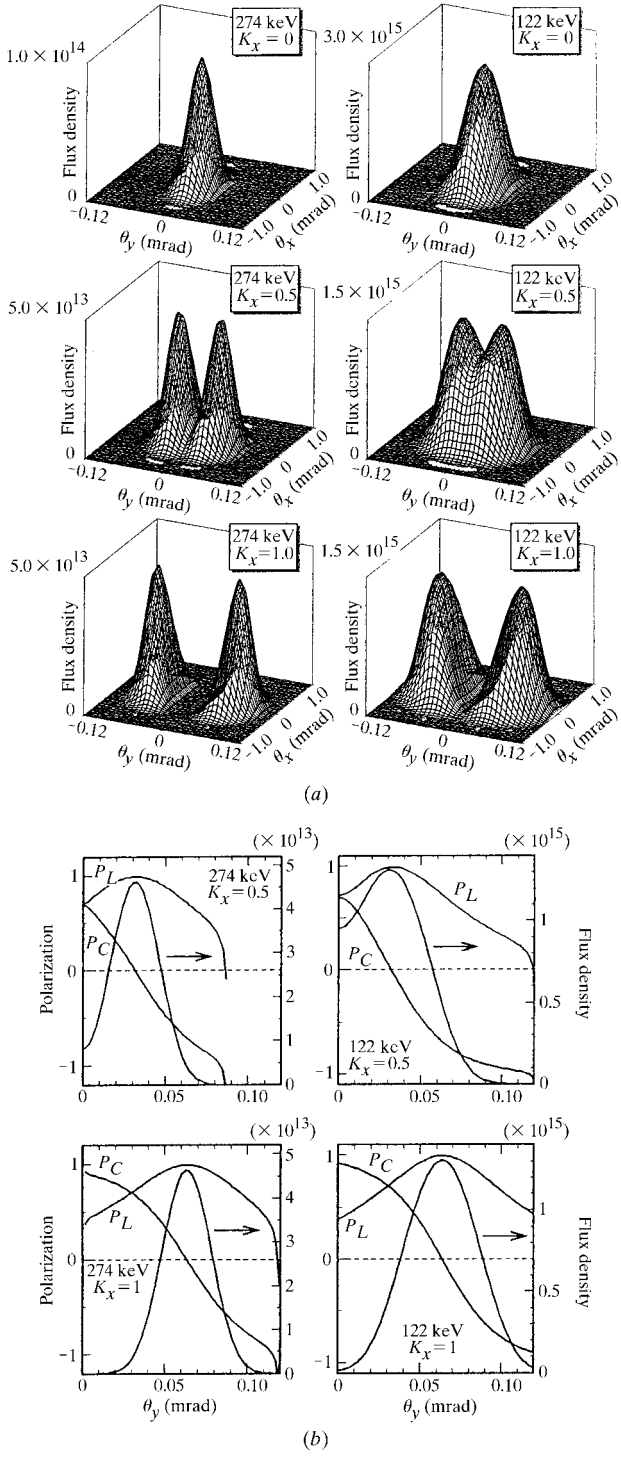

Figure 2
Distributions of (a) flux density $N_{\rm ph}$ and (b) Stokes parameters for linear polarization P_L and circular polarization P_C of X-rays emitted from the elliptical multipole wiggler. K_y is fixed at 9.894.

high along the z-axis, while P_L is high at the peaks. Fig. 3 shows the evaluated $h(\theta_H, -\theta_H, 90)$ as a function of θ_H and K_x. Numerical values of $N_{\rm ph}$, P_C and P_L were referred to a computer simulation performed using the program *SPring-8 spectra* (Tanaka & Kitamura, 1998). In the case of the 274 keV photon flux, as shown in Fig. 3, it was found that, for any K_x parameter greater than 0.3, the maximum of h is approximately the same, and the values $K_x = 1.0$ and $\theta_H = 0.057$ mrad were adopted. We can understand from Fig. 2(*b*) that the selected value of θ_H covers the flux density between the two peaks.

The following ratio $g(\theta_1,\theta_2, \theta)$ between the spin-dependent intensity and the total intensity is required later for comparison with experimental data,

$$g(\theta_1, \theta_2, \theta) = \Phi_2(\theta, \boldsymbol{\sigma}, \mathbf{k}_0, \mathbf{k}) \int_{-\infty}^{\infty} \mathrm{d}\theta_x \int_{\theta_2}^{\theta_1} N_{\rm ph}(\theta_x, \theta_y) P_C(\theta_x, \theta_y)\, \mathrm{d}\theta_y \Big/ \int_{-\infty}^{\infty} \mathrm{d}\theta_x \int_{\theta_2}^{\theta_1} N_{\rm ph}(\theta_x, \theta_y) \times \left[\Phi_0(\theta, E_0, E) + P_L(\theta_x, \theta_y)\Phi_1(\theta)\right] \mathrm{d}\theta_y \times (m_{\rm spin}/n_{\rm tot}). \quad (4)$$

Here $n_{\rm tot}$ denotes the total electron number per atom of the sample, and $m_{\rm spin}$ denotes the spin component of magnetization of the sample in units of the Bohr magneton, $\mu_{\rm B}$; the cross section of the magnetic Compton scattering does not depend on the orbital angular momentum (Lovesey, 1993; Sakai, 1994).

In addition to enhancing the spin-dependent Compton scattering intensity, a good momentum resolution for Compton-profile measurements is highly desired so that details of the momentum distribution of the electrons can be clarified. The momentum component p_z along the scattering vector can be experimentally evaluated by the equation

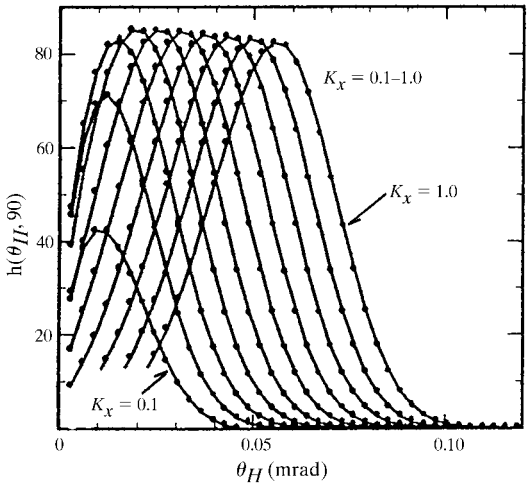

Figure 3
Calculated $h(\theta_H, 0, 90)$ for 274 keV X-rays as a function of K_x and θ_H.

$$p_z = \frac{E - E_0 + E_0 E(1 - \cos\theta)/mc^2}{\left(E_0^2 + E^2 - 2E_0 E\cos\theta\right)^{1/2}} mc. \quad (5)$$

Here the constant mc is 137.036 a.u. According to (5), a finite momentum resolution Δp_z is caused by the uncertainty of E_0, that of E arising from the energy resolution of a detector, and the divergence of θ,

$$\Delta p_z = \left[\left(\frac{\partial p_z}{\partial E_0}\Delta E_0\right)^2 + \left(\frac{\partial p_z}{\partial E}\Delta E\right)^2 + \left(\frac{\partial p_z}{\partial \theta}\Delta\theta\right)^2\right]^{1/2}, \quad (6)$$

with

$$\frac{\partial p_z}{\partial E_0} = \frac{-mcE\left[E_0 + E - E(E - E_0\cos\theta)/mc^2\right](1 - \cos\theta)}{(E_0^2 + E^2 - 2E_0 E\cos\theta)^{3/2}}, \quad (7)$$

$$\frac{\partial p_z}{\partial E} = \frac{mcE_0\left[E_0 + E + E_0(E_0 - E\cos\theta)/mc^2\right](1 - \cos\theta)}{(E_0^2 + E^2 - 2E_0 E\cos\theta)^{3/2}}, \quad (8)$$

$$\frac{\partial p_z}{\partial \theta} = \frac{mcEE_0\left\{E_0 - E + \left[E_0^2 + E^2 - E_0 E(1 + \cos\theta)\right]/mc^2\right\}\sin\theta}{(E_0^2 + E^2 - 2E_0 E\cos\theta)^{3/2}}. \quad (9)$$

The first and the third terms in (6) induce Compton-peak shifts of Compton profiles, and deteriorate a resultant momentum resolution. The first and second terms in (6) introduce the ambiguity of the scattering vector. Equations (7) and (8) indicate that the ambiguity of E_0 and E considerably worsens the momentum resolution when scattering angles are large. Equation (9) indicates that the influence of $\Delta\theta$ is most significant at $\theta = \pi/2$. Then, $\Delta\theta$ should be as small as possible to achieve a good momentum resolution for experiments with RSG.

It is important to compare the amount of the peak shift ΔE_θ caused by $\Delta\theta$ with the amount of the Doppler shift $\Delta E_{\rm D}$. The former can be evaluated by using (8) and (9) to be

$$\Delta E_\theta = \frac{\partial E}{\partial\theta}\Delta\theta = \left[\left(\frac{\partial p_z}{\partial\theta}\right)\Big/\left(\frac{\partial p_z}{\partial E}\right)\right]\Delta\theta = \frac{E\left[1 - \frac{E}{E_0} + \frac{E_0}{mc^2}\left\{1 - \frac{E}{E_0}(1 + \cos\theta) + \left(\frac{E}{E_0}\right)^2\right\}\right]\sin\theta}{1 + \frac{E}{E_0} + \frac{E_0}{mc^2}\left(1 - \frac{E}{E_0}\cos\theta\right)(1 - \cos\theta)}\Delta\theta, \quad (10)$$

and the latter is

$$\Delta E_D = \frac{E_0\left[1 + (E/E_0)^2 - 2(E/E_0)\cos\theta\right]^{1/2}}{1 + (E_0/mc^2)(1 - \cos\theta)}\frac{\Delta p_z}{mc}. \quad (11)$$

Fig. 4 shows the ratios, as a function of θ, between $\Delta E_{\rm D}$ for Δp_z = 1 a.u. and an instrumental resolution ΔE that consists of an energy resolution of a detector and ΔE_θ. When $\Delta\theta = 0$, it can be seen that the ratio $\Delta E_{\rm D}/\Delta E$ is more

enhanced at $\theta = \pi/2$ by higher-energy photons. This advantage is in agreement with the enhancement of the spin-dependent Compton scattering, and beneficial to measuring magnetic Compton profiles at $\theta = \pi/2$; it should be noted that this merit diminishes when $\Delta\theta$ becomes large, as demonstrated in Fig. 4.

3. Experimental details

Experiments using 274 keV and 122 keV photons have been carried out on station A and station B, respectively, at beamline BL08W of the SPring-8 facility, Japan. Fig. 5 shows the experimental set-up for 274 keV photons. The sample was a 5 mm-thick polycrystalline Fe plate incorporated into a C-type small electromagnet. According to (2), f for $\theta = 90^\circ$ is optimized when the magnetization, *i.e.* the spin direction $\boldsymbol{\sigma}$, is parallel to the scattered photon direction $\mathbf{k}$. This arrangement, however, causes the serious absorption of scattered photons by the Fe sample. The figure of merit f was then re-estimated by this sample absorption, and 31.3° was evaluated as the best angle between $\boldsymbol{\sigma}$ and $\mathbf{k}$. The Compton-scattered photons were detected by a Ge-SSD1 (Eurisys, EGPC 30-185-R: diameter 51.6 mm, thickness 66.6 mm) and a Ge-SSD2 (Canberra, GL0115: diameter 11.3 mm, thickness 15 mm) detector. The peak energy of the Compton profile was 178.4 keV. Ge-SSD1 has a good detection efficiency of about 70% at this energy, but its low-energy resolution gives a corresponding momentum resolution of 2.4 a.u. A relatively large angle divergence of 56.6 mrad was adopted in compliance with the detector resolution, and the $\Delta\theta$-dependent momentum resolution was 2.27 a.u. On the other hand, Ge-SSD2 has a detection efficiency of 49.7% and its energy resolution gives a momentum resolution of 0.33 a.u. An angular divergence $\Delta\theta = 9.5$ mrad was then adopted to realize a tolerable overall momentum resolution. The counting rate, however, was very low due to the low flux of 274 keV photons and the small scattering-angle allowance. Although the present result for Ge-SSD2 is not satisfactory in terms of the counting efficiency, the result suggests a further improvement in Δp_z of better than 0.4 a.u. if a smaller $\Delta\theta$ could be adopted. The observed energy spectra for $I_{\rm up} + I_{\rm down}$ and $I_{\rm up} - I_{\rm down}$ are shown in Fig. 6, where $I_{\rm up}$ and $I_{\rm down}$ correspond to the intensities of Compton profiles with a positive and negative magnetic field, respectively. The spin-dependent effect can be evaluated by the ratio $g = (I_{\rm up} - I_{\rm down})/(I_{\rm up} + I_{\rm down} - {\rm BG})$, where BG denotes the background intensity. This g ratio is equivalent to (4).

Similar measurements have been made using 122 keV photons and Ge-SSD2. The high photon flux density of 122 keV photons allowed a narrow width of the front-end slits to be used. The Compton-peak energy was 97.6 keV. The detector has 100% detection efficiency at this energy, and a reasonable energy resolution of the detector gives a momentum resolution of 0.42 a.u. at the Compton peak. The sample was a 2 mm-thick polycrystalline Fe plate and the magnetization direction was optimized at 31.1°. The

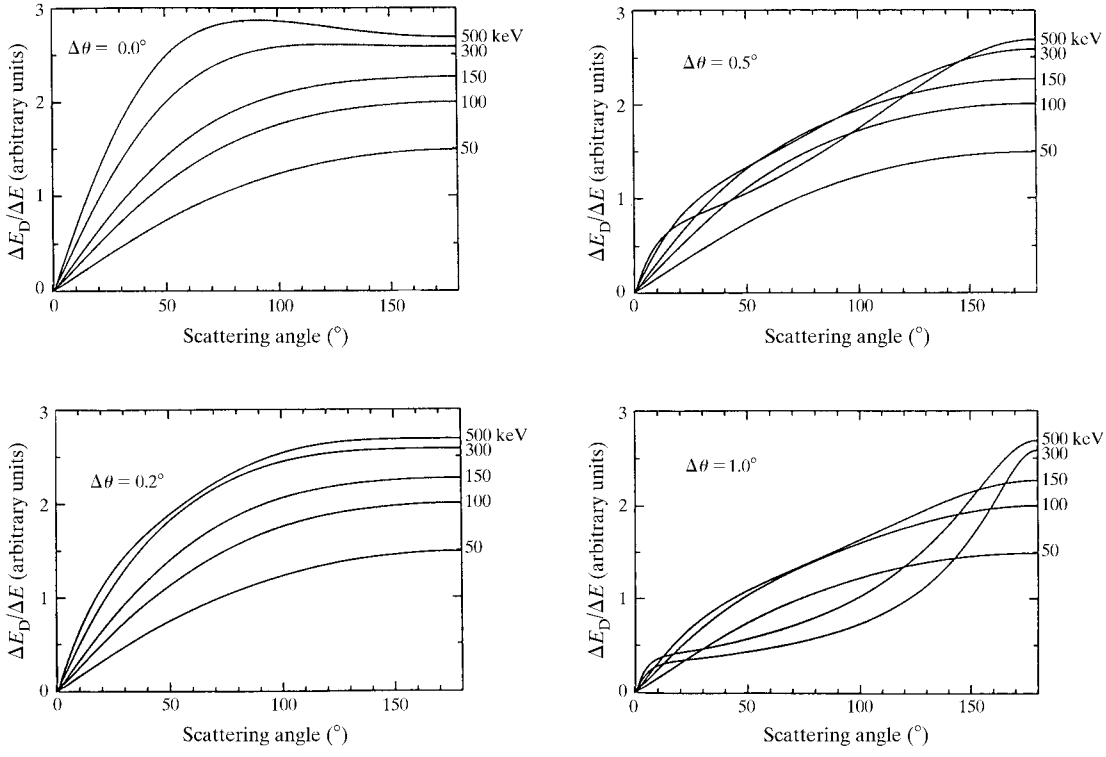

Figure 4
Ratios in arbitrary units between the Doppler broadening and an instrumental energy uncertainty ΔE as a function of the scattering angle θ and the scattering-angle divergence $\Delta\theta$.

beam spot at the sample position measured by a Polaroid film (Polapan 57) was 2 mm wide and 7 mm high. The distance between the sample and the detector was 175 cm, and a narrow slit of width 1 mm was placed in front of the detector. The resultant $\Delta\theta$ was 2.1 mrad. Since the flux of 122 keV photons is about 10^3 times higher than that of 274 keV photons, the optimized condition for θ_H evaluated by (3) induced a tremendous amount of scattered photons, causing the Ge detector to overload: the dead time of the electronics for the energy analysis increased almost up to 100%. Then the front-end slit was crucially collimated to 3.06 μrad at θ_1 = 0.041 mrad, which selects the best polarization parameters, as shown in Fig. 7, and the monochromated photon flux was adjusted to an adequate intensity for the detector system. The factor m_{mag} in equation (4) was experimentally evaluated from the magnetization of the sample: m_{mag} = 2.07 for a 2 mm-thick Fe sample and m_{mag} = 1.87 for a 5 mm-thick sample, each of which was measured by winding a 25 turn pick-up coil around the sample and connecting it to a flux meter; here the orbital magnetic moment of Fe is neglected. The reduction of m_{mag} for the thicker sample indicates incomplete magnetization of the sample.

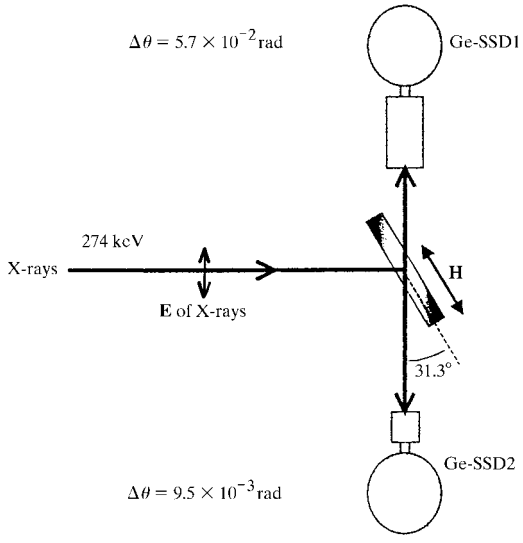

Figure 5
Experimental set-up for 274 keV X-rays. The linear polarization vector is in the scattering plane, giving $P_L \simeq -1$.

4. Results and conclusion

The experimental results are summarized in Table 1. The experimental g ratios are compared with the theoretical ones. Good agreement is found within the experimental errors, which are mainly due to the ambiguity of the background subtraction. As may be seen from Table 1 for $\Delta p_z(E_0)$, which directly reflects the accuracy of E_0, a single bent monochromator for 274 keV X-rays gives a good energy resolution $\Delta E_0/E_0$ better than 10^{-3}, while that for 122 keV X-rays was not so good. This was simply due to a tentative adjustment of a doubly bent monochromator for 122 keV X-rays. The highest g ratio, 3.4%, is observed for

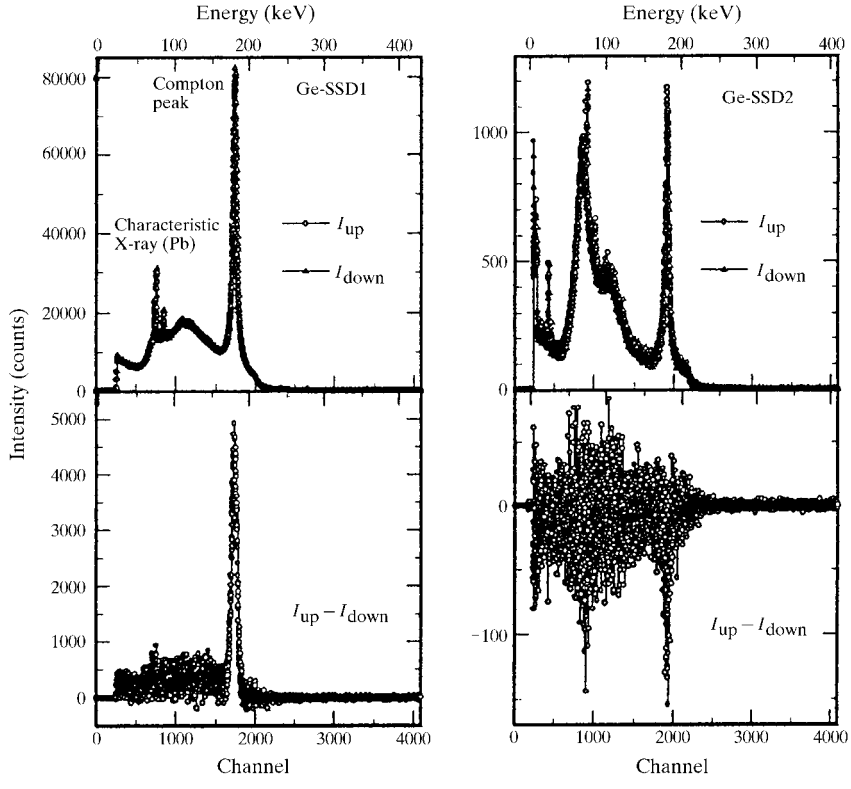

Figure 6
Experimental total and magnetic Compton profiles measured using Ge-SSD1 and Ge-SSD2. The incident energy is 274 keV.

Table 1
Experimental results and theoretical estimation.

The g ratio of experiment 2 is eliminated because of its low statistical accuracy.

Item	Experiment 1	Experiment 2	Experiment 3
Accumulation time for $I_{up} + I_{dwn}$ (h)	44.3	44.3	29.4
Count rate under Compton line (s^{-1})	104	1.37	858
Detector	Ge-SSD1	Ge-SSD2	Ge-SSD2
E_0 (keV)	274	274	122
θ (°)	90	90	90
g (experiment) (%)	3.2 ± 0.5	–	3.38 ± 0.35
g (theory) (%)	3.52	3.52	3.49
$\partial p_z/\partial\theta$ (a.u. rad^{-1})	40.08	40.08	20.25
$\Delta\theta$ (mrad)	56.6	9.5	2.1
$\Delta p_z(\Delta\theta)$ (a.u.)	2.27	0.382	0.0425
$\Delta p_z(\Delta E)$ (a.u.)	0.795	0.327	0.423
$\Delta p_z(\Delta E_0)$ (a.u.)	<0.01	<0.01	0.458
Δp_z (a.u.)	2.41	0.503	0.625

122 keV photons. This ratio is better than the best value for BSG of 2.4% at BL08W. From the viewpoint of the statistical accuracy, this enhancement is equivalent to twice the reduction of the accumulation time. If the flux density of the 274 keV photons increased comparably with that of the 122 keV photons, the front-end slits could be narrowed, and the g ratio for the 274 keV photons would become 5%, because the ratio $\Phi_2/(\Phi_0 + P_L\Phi_1)$ is increased with increasing photon energy.

A shallow dip at the top of the magnetic Compton profile in Fig. 8 measured by using 122 keV X-rays together with Ge-SSD2 clearly demonstrates that the RSG method also guarantees a good momentum resolution comparable with the BSG method (Sakai, 1996; McCarthy *et al.*, 1997). If the flux density of the 274 keV photons could be increased, it would be possible to improve $\Delta p_z(\Delta\theta)$ by using a narrower slit, and an overall momentum resolution better than 0.4 a.u. could be achieved.

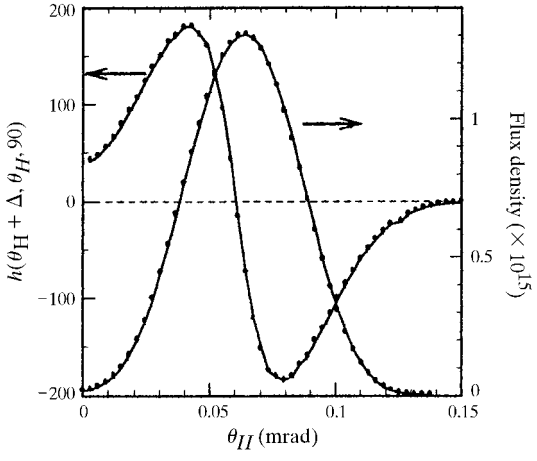

Figure 7
$h(\theta_H + \Delta, \theta_H, 90)$ and flux density distributions for 122 keV X-rays and K_x = 1.0 with a slit width Δ = 3.06 μrad.

According to Φ_2 in (1), the spin direction is desirable to be parallel to the direction of the vector $\mathbf{k}_0\cos\theta + \mathbf{k}$. In the case of BSG, the direction of this vector can be approximated by the scattering vector $\mathbf{K} = \mathbf{k}_0 - \mathbf{k}$. Then the z-axis ($z\|\mathbf{K}$) and an applied magnetic field are required to be approximately parallel. Since the direction of $\mathbf{K}$ is roughly approximated by $\mathbf{k}_0$, the shape of a sample for magnetic Compton-profile measurement is usually prepared to be long in the direction along the incident photon in consideration of the demagnetization effect. In addition, the large magnetic anisotropy sometimes makes it difficult to magnetize a single crystalline sample in the best direction. RSG experiments allow a large angle between the z-axis and the applied magnetic field, providing a degree of freedom to the experimental set-up. Suppose we use a disc as a sample, and magnetize it (the direction of $\boldsymbol{\sigma}$) parallel to the surface. When the incident energy is 120 keV, the angle between the incident X-rays and the z-axis is 39°. If we set the sample surface at an angle of 51° off the incident direction, the direction of the z-axis can be perpendicular to the applied magnetic field.

The authors gratefully acknowledge Dr Y. Sakurai, Dr J. Mizumaki and Dr M. Itoh of the Japan Synchrotron Radiation Research Institute for their help and advice at BL08W of SPring-8. This research was performed under the SPring-8 approval numbers 1998A0122-NM-np and 1999A0141-CD-np.

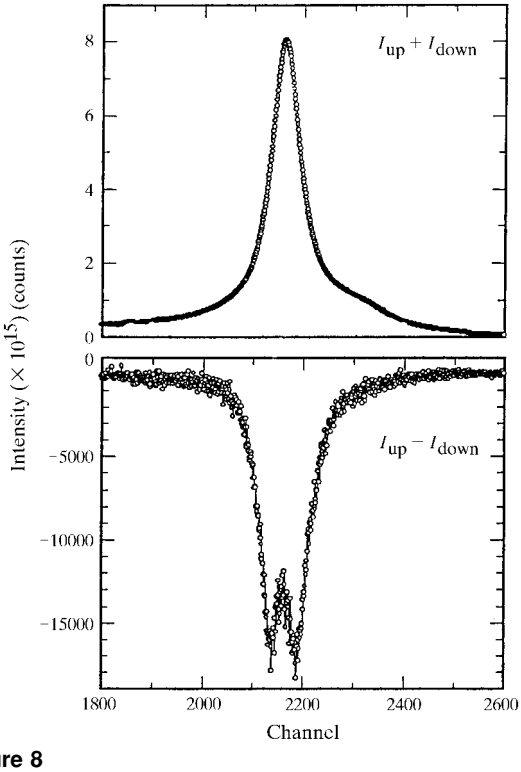

Figure 8
Experimental total and magnetic Compton profiles measured using Ge-SSD2. The incident energy is 122 keV.

References

Brunel, M., Patrat, G., de Bergevin, F., Rousseaux, F. & Lemonnier, M. (1983). *Acta Cryst.* A**39**, 84–88.
Ito, M. & Hirano, H. (1997). *J. Phys. Condens. Matter*, **9**, L613–L618.
Lipps, F. W. & Tolhoek, H. A. (1954). *Physica*, **20**, 85–98; 395–404.
Lovesey, S. W. (1993). *Rep. Prog. Phys.* **56**, 257–326.
McCarthy, J. E., Cooper, M. J., Lawson, P. K., Timms, D. N., Manninen, S. O., Hamalainen, K. & Suortii, P. (1997). *J. Synchrotron Rad.* **4**, 102–109.
Sakai, N. (1994). *J. Phys. Soc. Jpn*, **63**, 4655–4656.
Sakai, N. (1996). *J. Appl. Cryst.* **29**, 81–99.
Tanaka, T. & Kitamura, H. (1998). http://radiant.harima.riken.go.jp/specra/index_e.html